Supplement of Hydrol. Earth Syst. Sci., 29, 5625–5644, 2025 https://doi.org/10.5194/hess-29-5625-2025-supplement © Author(s) 2025. CC BY 4.0 License.





Supplement of

Linking chemical weathering, evolution of preferential flow paths and transport self-organization in porous media using non-equilibrium thermodynamics

Evgeny Shavelzon et al.

Correspondence to: Evgeny Shavelzon (evgeny.shavelzon@gmail.com) and Yaniv Edery (yanivedery@technion.ac.il)

The copyright of individual parts of the supplement might differ from the article licence.

S1. Lagrangian particle tracker validation in 2D

20

Lagrangian particle tracking (LPT) approach is employed in the current study to model the dynamic evolution of the coupled reaction-transport process in heterogeneous porous media, representative of chemical weathering. The solute transport in the medium is simulated by injecting a statistical ensemble of particles in the medium, their motion governed by the Langevin stochastic differential equation. We discretize the Langevin equation using the simple Euler-Maruyama method to be used in the context of a numerical simulation (Kloeden (1992)). To validate the LPT model against a known analytical solution, we employ the well-known equivalence property between the statistical ensemble of particles governed by the Langevin equation and the solution of the advection-diffusion equation (Risken (1996), Perez et al. (2019)).

We consider the two-dimensional scenario of solute injection into a medium characterized by uniform transport properties, governed by a steady state flow, for which the analytical advection-diffusion equation solution for the spatial distribution of solute concentration is given by the bivariate Gaussian bell (Kreft and Zuber (1978)). In the instantaneous injection case, the variance of the concentration distribution is $\sigma = \sqrt{2Dt}$ in both dimensions, where D is the diffusion coefficient and t is the time since the injection, and the expectation $\mu = vt$ in the direction of the flow equals to the extent by which the flow of speed v has advanced in the length of time t, while the expectation in the transverse direction is zero (Kreft and Zuber (1978)). This reflects the obvious notion that the solute transport in the direction of the flow is governed by both advection and diffusion, while in the transverse direction only diffusion is responsible.

For model verification, a total of 1e5 particles were injected into the field characterized by a homogeneous hydraulic conductivity $k_0 = 0.39$ [cm/min] and porosity $\theta_0 = 0.43$, and a steady state flow along the X direction, obtained by applying a hydraulic head gradient $\Delta h = 100$ [cm] between the inlet and outlet of the field. A diffusion coefficient of D = 1.0e-5

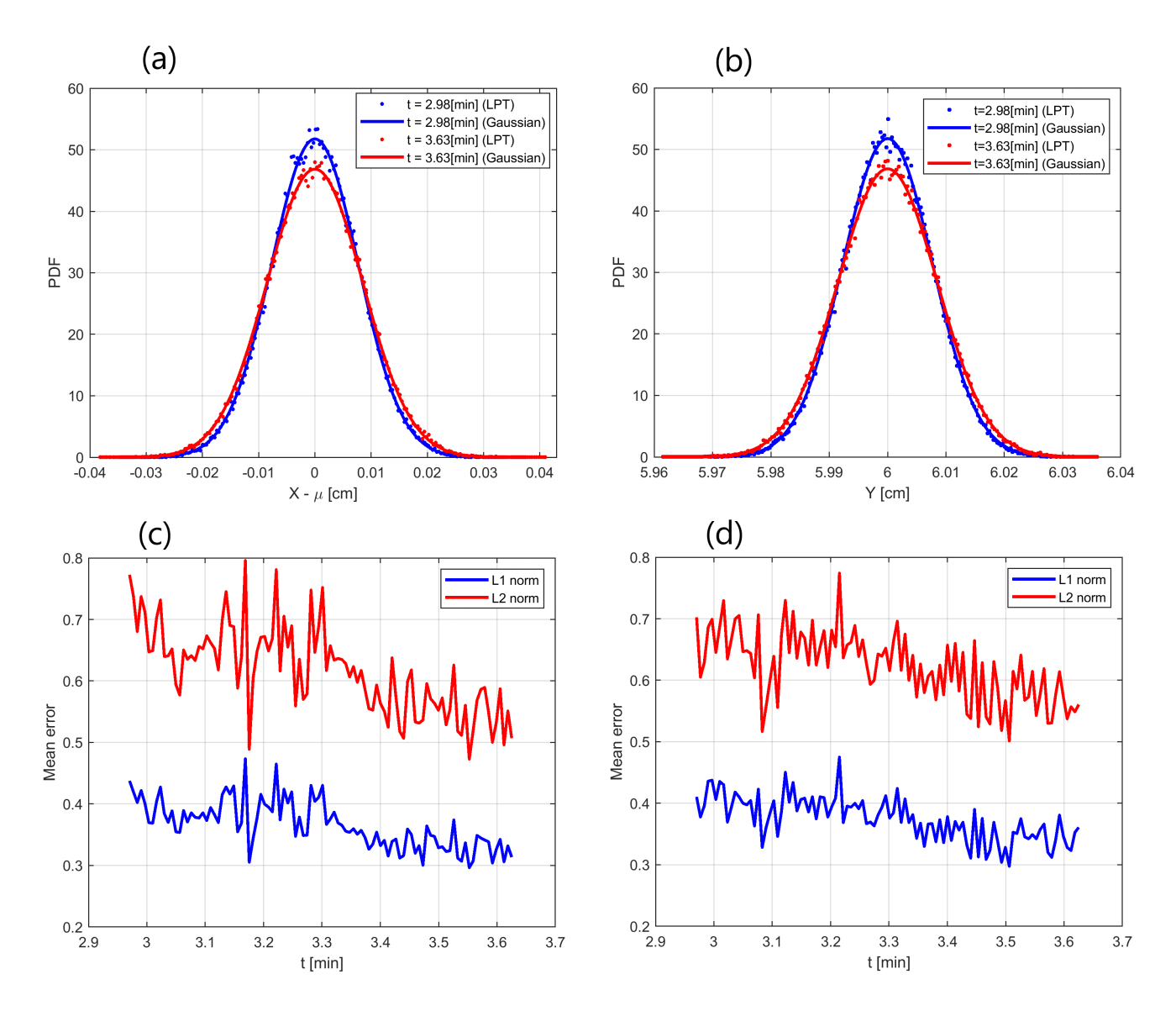


Figure S1. Verification of the Lagrangian particle tracker model against the 2D advection-diffusion solution for the case of injection into a medium, characterized by uniform transport properties and governed by a steady-state flow: (a) Spatial distribution in the X direction at t = 2.98, 3.63[min] as a function of $X - \mu$, (b) Spatial distribution in the Y direction at t = 2.98, 3.63[min] as a function of Y (c) Mean error between the normalized spatial distributions in the X direction obtained from LPT and ADE in L_1 , L_2 norms as a function of time and (d) Mean error between the normalized spatial distributions in the Y direction, obtained from LPT and ADE, in L_1 , L_2 norms as a function of time. Dot markers show LPT data while solid lines represent the advection-diffusion equation solution.

[cm2/min] was employed. For verification, we compared the particles spatial distribution, obtained from LPT simulations, to the analytical solution of the advection-diffusion equation. The spatial distributions of the injected particles along the flow and

transverse directions (X and Y, respectively) were converted into the probability density functions (PDF) by normalization, which were then compared to the corresponding Gaussian distributions.

Figure S1 shows the results of the Lagrangian particle tracker validation using the two-dimensional ADE analytical solution for instantaneous injection into a homogeneous medium governed by a steady-state flow. Frames (a) and (b) present the normalized particle spatial distributions in the X and Y directions at times t = 2.98, 3.63[min] (dot markers show particle tracking data while solid lines show the analytical ADE solution, notice also that the X-distribution is shown as a function of $X - \mu$ to account for the advective motion). Frames (c) and (d) present the Mean error between the normalized spatial distributions in the X and Y directions, obtained from LPT and ADE, in L_1, L_2 norms as a function of time. Good agreement between LPT and the advection-diffusion equation is clear, although some inevitable fluctuations in the LPT data are present.

S2. Non-equilibrium thermodynamics in a nutshell

A non-equilibrium system is, as the name implies, a system that is not in thermodynamic equilibrium. In such a system gradients of the thermodynamic state properties such as temperature, pressure and concentration of chemical species are present, as opposed to a system in equilibrium where these properties are homogeneous throughout. The presence of gradients in thermodynamic potentials such as pressure, temperature and chemical potential implies a net transfer of energy or matter, or thermodynamic flux, within the system or across its boundaries. Examples include heat transfer, where heat flux travels in the medium due to applied temperature gradient, hydrodynamic flow where mass flux is driven by hydraulic head gradient, mixing of chemical species and chemical reaction, both driven by the gradient of chemical potential (see left column in Figure S2). All of these processes may be seen as dissipative, meaning that the free, or useful energy in the system (energy available to perform useful work, for example internal, kinetic or potential) is being expended, since energy must be constantly supplied to the system in order to maintain these fluxes. Obviously, free-energy of the system is not a conserved property. A system that receives influx of energy from surroundings is said to be an open system, as it interacts with surroundings. Such a system may be maintained in a non-equilibrium thermodynamic stationary state of constant thermodynamic flux. On the other hand, a system without constant supply of energy from outside will soon deplete its available free-energy, reducing its capacity to do thermodynamic work and leading to a decline in the thermodynamic potential gradient and, therefore, cessation of the resulting thermodynamic flux. Such a system is found in a state of equilibrium, characterized by homogeneity in thermodynamic state properties (see right column in Figure S2). Thus, to maintain mass flux of a fluid through a pipe, a constant hydraulic head gradient must be maintained between the pipe ends to overcome viscous frictional effects and gravitational head differences. This can be done by operating a pump that maintains the head gradient and, thus, the mass flow in a pipe by consuming electrical power. Should the supply of electrical power to the pump cease, the head gradient will no longer be maintained and, at some point, the mass flow through the pipe will stop, as the available free-energy in the system has been depleted by viscous dissipation. Thus, such a process is clearly a dissipative one.

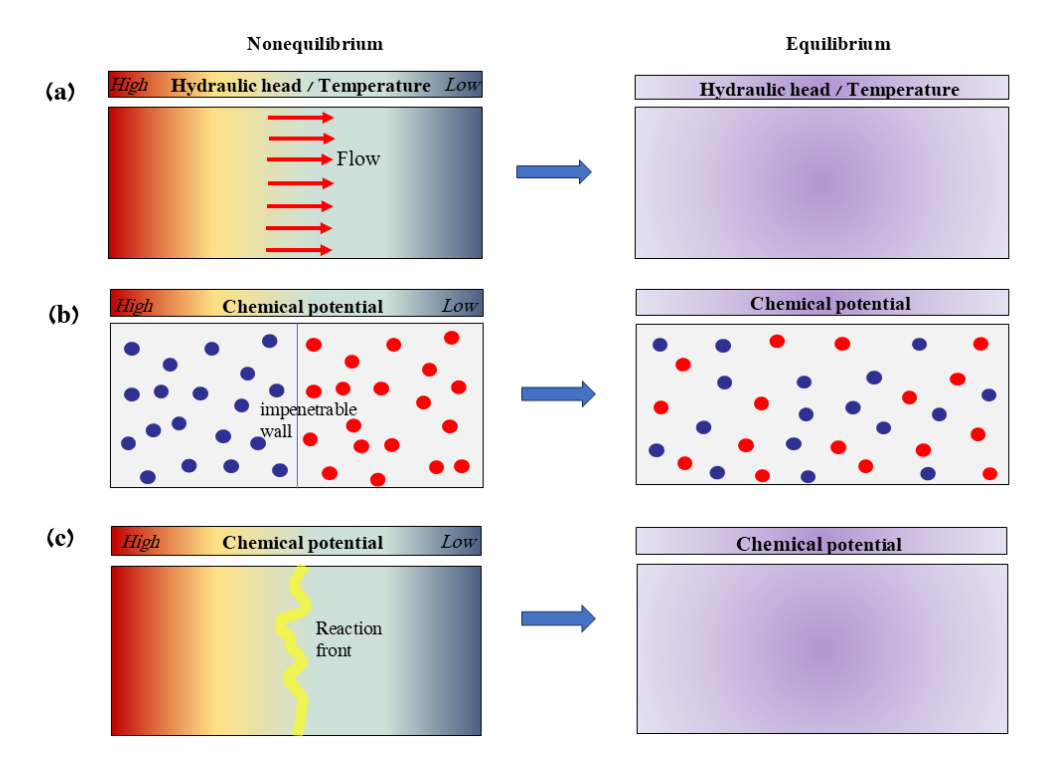


Figure S2. Examples of non-equilibrium processes (left column) and systems in equilibrium (right column) in (a) heat transfer and hydrodynamic flow, (b) mixing of chemical species and (c) chemical reaction.

An important outcome of non-equilibrium thermodynamics is that dissipative irreversible processes produce entropy at a rate that is directly related to the power dissipated during the process, the proportionality constant between them being the local temperature (see Section 3.1 in the manuscript). Here, an assumption of *local equilibrium* is required, implying that a non-equilibrium system still experiences equilibrium, albeit on a local scale. Thus, instead of a homogeneous temperature that characterizes system in equilibrium, in a non-equilibrium system we may assume that each small volume of the system is locally in equilibrium, thus temperature (and other thermodynamic state variables) can be defined locally. This results implies that, by studying entropy generation due to various dissipative processes pertinent to the non-equilibrium system under consideration, important observations can be made regarding the dynamics of its physical behavior. Thus, a decrease in entropy production means that the process now occurs in a more efficient way, with less useful energy depleted per unit of transferred thermodynamic flux.

When applying the non-equilibrium thermodynamic framework to the problem of reactive flow in porous media characteristic of geochemical weathering, where dissolution-precipitation of the porous matrix takes place, it is natural to concentrate on the following interrelated processes: (a) *percolation*, or fluid transport through the porous matrix, which involves dissipation of hydraulic power while overcoming the hydraulic resistance of the matrix due to viscous friction effects, affects concentration

distribution of the chemical species and, therefore, directly influences chemical reaction, (b) *mixing* of chemical constituents that involves dissipation of chemical energy and affects the reaction rate and (c) *chemical reaction* of dissolution-precipitation, also involving dissipation of chemical energy, which affects directly the transport through matrix. For further details regarding non-equilibrium thermodynamics see, for instance, Kondepudi and Prigogine (1998).

S3. Calculation of entropy generation terms

Percolative entropy. The percolative entropy generation term, reprinted from (20), is given by

80
$$\sigma_{perc} = -\frac{\nabla p}{T} \cdot \sum_{i} v_{i} \mathbf{J}_{i}$$
 (S1)

Our computational model for reactive flow and transport in porous media (eqs. (1)–(2) in the manuscript) is built upon linear fundamental laws. In general, not too far from equilibrium, the thermodynamic flux J_i can be written as a linear combination of thermodynamic forces (Onsager, 1931)

$$\mathbf{J}_i = \sum_j L_{ji} \mathbf{F}_j \tag{S2}$$

where \mathbf{F}_j are the forces and L_{ji} are the phenomenological constants. The expression (S2) implies, in general, that a thermodynamic force can not only drive the corresponding flux (such as the temperature gradient that drives the heat flux), but also affect other fluxes. Consider, as an example, the thermoelectric effect, where the thermal gradient drives not only the heat flux but also an electrical current and vice versa (Kondepudi and Prigogine, 1998). This type of coupling between various thermodynamic forces is called a cross effect. The ensuing Onsager reciprocal relations (Onsager, 1931) form the basis for the linear regime of non-equilibrium thermodynamics. In the specific case of percolative entropy, the thermodynamic force represented by the pressure gradient drives the mass flux in the field. We neglect the cross effects, as the reactive process cannot affect the convective flow because of the symmetry principle stating that a scalar thermodynamic force with high degree of isotropy, such as the partial molar Gibbs energy, cannot affect the vectorial convective flux that has lower isotropy due to its directionality; the diffusive effects can be easily neglected as well by the same reasoning (Kondepudi and Prigogine, 1998). We employ the Darcy's law (2) to obtain the relation between the convective flux \mathbf{q} and the pressure gradient (here the relation is brought in the pressure form, as opposed to the hydraulic head form used previously)

$$\mathbf{q} = -K' \, \nabla p \tag{S3}$$

where $K' = K/\rho g$ is the hydraulic conductivity of the porous medium that corresponds to the pressure form of Darcy's law (S3). Notice that the sum of molar fluxes given in the laboratory frame of reference, multiplied by the specific molar volumes, is exactly the total Darcy flux in a volume element $\mathbf{q} = \sum_{i} v_i \mathbf{J}_i$. Substituting the latter relation into (S3) and (S1) and multiplying by the volume of a computational cell per unit depth $\Delta x \Delta y$, which we consider to be the elementary volume in our numerical implementation, we obtain the percolative entropy generation rate in a single computational cell

$$T\sigma_{perc} = K'(\nabla p)^2 \Delta x \Delta y \tag{S4}$$

Notice that the resulting formula is identical to the hydraulic work dissipated as the fluid moves through the cell, overcoming the hydraulic resistance of the porous medium. This result can be seen as a private case of the Gouy-Stodola theorem Gouy, 1889 that links the rate of destruction of the available energy in a system to the rate of entropy generation. Since entropy is an extensive property, the total percolative entropy generation in the field $\dot{S}_{gen,perc}$ can be obtained by integrating (S4) over the volume of the computational field V, which amounts to summing the contributions of all computational cells

$$T\dot{S}_{gen,perc} = \int_{V} T \sigma_{perc} = \sum_{i,j} (T \sigma_{perc})_{i,j}$$
 (S5)

Here i,j are the cell indices in the x- and y directions, respectively. Since the statistical realizations of the heterogeneous computational field, generated using the SGSIM code, exhibit significant deviations in the mean hydraulic conductivity value for different heterogeneity values, this will inevitably lead to deviations in the total flow rate in the field when solving for the flow field for different realizations (recall the applied boundary conditions of constant hydraulic head drop over the field). To account for these deviations, we normalize the expression for the total percolative entropy generation rate $T\dot{S}_{gen,perc}$ by the quantity $T_{ref}R\dot{N}_{tot}$, where T_{ref} is the reference temperature taken to be 293.15K, R is the universal gas constant and \dot{N}_{tot} is the total molar flow rate into the field. The obtained dimensionless quantity $\dot{S}_{gen,perc}/(R\dot{N}_{tot})$ represents the total percolative entropy generation rate in the field per unit flow rate of the incoming flow.

Reactive entropy. The reactive entropy generation term, reprinted from (20), is given by

120
$$\sigma_{react} = -\sum_{j} \frac{\Delta g_j}{T} \frac{d\xi_j}{dt}$$
 (S6)

For simplicity, we assume that reaction in a computational cell occurs under conditions of perfect mixing in a cell; thus diffusive cross-effects in a cell are not important. The total amount of reaction in a cell during the computational time step Δt is calculated based on the distance from chemical equilibrium, defined by the current disposition of chemical species in the cell, as represented by the number of H^+ , H_2CO_3 particles there (see Section 2.3). In our model, a single global reaction of calcite dissolution/precipitation (7) is present. We denote its partial molar Gibbs energy as Δg . Since we neglect heat transfer effects in the current study, we consider the reactive entropy generation as an indicator of the intensity of the chemical reaction. We assume linear relation between Δg and $\frac{d\xi}{dt}$ in the vicinity of chemical equilibrium

$$\frac{d\xi}{dt} = -\frac{r_{f,eq}}{RT}\Delta g\tag{S7}$$

where $r_{f,eq}$ is the forward reaction rate in equilibrium (see Chapter 9 in Kondepudi and Prigogine, 1998), and define the extent of reaction as $\frac{d\xi}{dt} = \frac{dc_{H^+}}{dt} = \frac{M_{H^+}}{\Delta x \Delta y} \frac{dN_{H^+}}{dt}$, where M_{H^+} is the molar parcel assigned to a single H^+ particle, c_{H^+} is the molar concentration of H^+ in the cell, $\Delta x \Delta y$ denotes the cell volume per unit depth and $\frac{dN_{H^+}}{dt}$ is the rate of conversion of H^+ particles into H_2CO_3 during the computational time step Δt . Notice that dc_{H^+} is the increment in the H^+ concentration in the computational cell due to reaction, necessary to achieve chemical equilibrium there. To obtain the expression for the reactive entropy generation rate in a computational cell, we employ (S7) in (S6) and multiply by the cell volume $\Delta x \Delta y$

135
$$\sigma_{react} = \frac{R}{r_{fea}} \left(\frac{dc_{H^+}}{dt}\right)^2 \Delta x \Delta y$$
 (S8)

To obtain the total reactive entropy generation in the field, we integrate (S8) over the volume of the computational field V, which amounts to summing the contributions of each computational cell.

$$\dot{S}_{gen,react} = \int_{V} \sigma_{react} = \sum_{i,j} (\sigma_{react})_{i,j}$$
 (S9)

Here i,j are the cell indices in the x- and y directions, respectively. Notice that the reactive entropy generation is directly related to the number of reactive events that have occurred in the field during the time interval Δt to reach chemical equilibrium cell-wise. Here, as well, we normalize the reactive entropy generation by the quantity $T_{ref} R \dot{N}_{tot}$. The obtained dimensionless quantity $\dot{S}_{gen,react}/(R \dot{N}_{tot})$ represents the total *reactive* entropy generation rate in the field per unit flow rate of the incoming flow.

145 Mixing entropy. The mixing entropy generation term, reprinted from (20), is given by

$$\sigma_{mix} = -\sum_{i} \frac{(\nabla \mu_i)_{T,p}}{T} \cdot \mathbf{J}_i \tag{S10}$$

To assess the evolution of the mixing entropy generation in the field subject to reaction-transport interaction, without taking into account chemical reaction, we consider the physical scenario of mixing of two non-reactive species, such as water and a non-reactive tracer. This scenario corresponds to a numerical setting of a non-reactive tracer test (NRPT), as described in Shavelzon and Edery, 2024, where the injected particles traverse the field subject to the laws described in Section 2 without chemical reaction. For mixing entropy calculation we employ the *cumulative* concentration distribution of the non-reactive tracer across the field, calculated by counting the total number of particles that visited each computational cell (see Shavelzon and Edery, 2024 for details). Mixing entropy, obtained from NRPT simulations, can be considered an auxiliary parameter that quantifies dispersivity in the field, therefore representing the thermodynamic counterpart to the Shannon entropy of transport self-organization that was also calculated from the concentration distribution of reactants.

We consider the mixing entropy generation in a single computational cell. For this scenario, we write the Gibbs-Duhem relation, assuming negligible deviations in pressure ans temperature across the cell

$$c_w(\nabla \mu_w)_{T,p} + c_{tr}(\nabla \mu_{tr})_{T,p} = 0$$
 (S11)

where the indices w, tr represent water and tracer, respectively. Another useful relation, that describes zero change in the volume of a fluid element due to diffusion, is given by

$$\frac{\mathbf{J}_w}{\rho_w} + \frac{\mathbf{J}_{tr}}{\rho_{tr}} = 0 \tag{S12}$$

where ρ_w , ρ_{tr} are the densities of water and tracer, respectively. These relations show that the thermodynamic forces, as well as the fluxes, are not independent in our scenario. Using (S11)–(S12), we are able to write the mixing entropy generation rate

165 as

150

$$\sigma_{mix} = -\frac{1}{T} \left(1 + \frac{c_{tr} \rho_w}{c_w \rho_{tr}} \right) \mathbf{J}_{tr} \cdot (\nabla \mu_{tr})_{T,p}$$
(S13)

Recalling that in the linear regime the thermodynamic fluxes can be written as a linear combination of the forces, as stated in (S2), we have

$$\mathbf{J}_{tr} = -\frac{L_{11}}{T} \left(1 + \frac{c_{tr} \, \rho_w}{c_w \, \rho_{tr}} \right) (\nabla \mu_{tr})_{T,p} \tag{S14}$$

where L_{11} is the phenomenological coefficient. By comparing (S14) with the Fick's law $\mathbf{J}_{tr} = -D\nabla c_{tr}$, where D is the diffusion coefficient of tracer in water, we may write

$$D = \frac{L_{11}}{T} \left(1 + \frac{c_{tr} \rho_w}{c_w \rho_{tr}} \right) \frac{\partial \mu_{tr}}{\partial c_{tr}}$$
 (S15)

Assuming that the mixed species behave as an ideal solution, where each component independently obeys the Raoult's law, the chemical potential of the tracer at temperature T and pressure p is given by Atkins and De Paula, 2006

175
$$\mu_{tr} = \mu_{tr}^0 + RT \ln \chi_{tr}$$
 (S16)

where μ_{tr}^0 is the standard chemical potential at T,p (standard state being pure liquid), R is the universal gas constant and $\chi_{tr} = c_{tr}/c_{tot}$ is the tracer molar fraction. For a dilute solution where $c_{tr} \ll c_w$, we have $\chi_{tr} = c_{tr}/c_w$ and

$$D = \frac{L_{11}R}{c_{tr}} \tag{S17}$$

By rewriting the chemical potential definition (S16) in terms of tracer concentration c_{tr} , substituting (S14), (S16) and (S17) into (S13) and multiplying by the volume of a computational cell $\Delta x \Delta y$, we obtain the entropy generation due to mixing of non-reactive tracer with water in a single computational cell

$$\sigma_{mix} = \frac{L_{11}}{T^2} \left(1 + \frac{c_{tr} \rho_w}{c_w \rho_{tr}} \right)^2 (\nabla \mu_{tr})_{T,p}^2 \Delta x \Delta y = \frac{DR}{c_{tr}} (\nabla c_{tr})^2 \Delta x \Delta y$$
 (S18)

The total mixing entropy generation in the field can be obtained by integrating (S18) over the volume of the computational field V, which amounts to summing the contributions of each computational cell

185
$$\dot{S}_{gen,mix} = \int_{V} \sigma_{mix} = \sum_{i,j} (\sigma_{mix})_{i,j}$$
 (S19)

Here i, j are the cell indices in the x- and y directions, respectively.

S4. Statistical analysis of the transport properties of the porous medium

We examine the evolution of the hydraulic conductivity field K, influenced by the coupled reactive-transport process. Figure S3a presents the evolution of the Relative mean value of hydraulic conductivity $\tilde{K} - \tilde{K}_0$ over the computational field, where \tilde{K}_0 is the initial mean conductivity value, as a function of dimensionless time \tilde{t} for varying σ_0^2 values (for each σ_0^2 , an ensemble average of 20 realizations). Here, the first 10 columns of computational cells near the inlet were excluded from the calculation due to the existence of a dissolution area there, which suppresses the reaction dynamic. Clearly, the constant influx of the

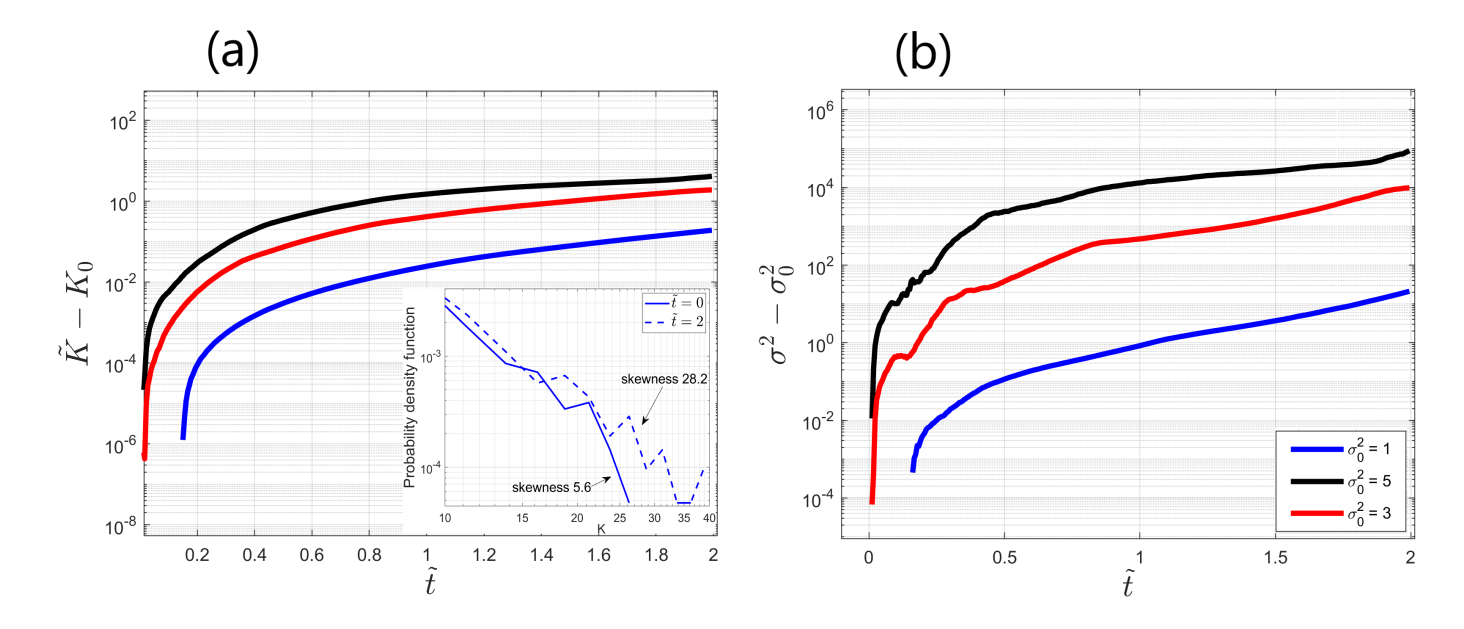


Figure S3. Evolution of the hydraulic conductivity distribution in the field over time: (a) Relative mean $\tilde{K}-K_0$ as a function of dimensionless time \tilde{t} (inset shows the tail of the probability density function for a single realization of the hydraulic conductivity distribution for $\sigma_0^2=1$ at times $\tilde{t}=0,2$, skewness values indicated with arrows) and (b) Relative variance $\sigma^2-\sigma_0^2$ as a function of dimensionless time \tilde{t} (ensemble average of 20 realizations).

195

200

205

 H^+ particles at the inlet of the field causes considerable dissolution, a significant part of which occurs in the preferential flow paths, as $\tilde{K} - \tilde{K}_0$ grows monotonously with \tilde{t} . The mean hydraulic conductivity curves for all σ_0^2 values assume a power law shape after enough particles have invaded the field to create a considerable statistical ensemble. The shape of the curves for different σ_0^2 values hints at the possibility of scalability with the variance of the conductivity field σ_0^2 , similar to Peclet number scaling achieved in Shavelzon and Edery, 2024. We observe that the mean conductivity value grows faster for more heterogeneous fields, as represented by higher values of σ_0^2 . This can be explained by the fact that for higher σ_0^2 the phenomenon of preferential flow paths becomes more dominant, thus leading to higher concentrations of the injected H^+ particles moving along these paths. This causes more dissolution inside these paths, thus contributing to faster growth of the mean conductivity value. The inset in Figure S3a shows the tail of the probability density function for a single realization of the hydraulic conductivity distribution for $\sigma_0^2 = 1$ at times $\tilde{t} = 0, 2.0$. The corresponding skewness values are indicated with arrows. Note that the hydraulic conductivity distribution is initially non-Gaussian and positively skewed, since the distributions obtained from SGSIM are considered as the natural logarithm of the hydraulic conductivity distribution in the field (see Section 2.1). The skewness of the conductivity distribution increases with time, which is exhibited by some "fattening" of the probability density function, as well as the longer and heavier tail on the right. This can be interpreted as an appearance of high conductivity regions due to intense dissolution reaction that occurs within the preferential flow paths. Similar tendencies are presented in Figure S3b, that shows the Relative hydraulic conductivity variance $\sigma^2 - \sigma_0^2$ as a function of dimensionless time \tilde{t} . We

observe that $\sigma^2 - \sigma_0^2$ exhibits a constant increase with dimensionless time \tilde{t} , as the particles advance and react in the field. The Relative variance of conductivity grows faster for higher values of σ_0^2 . This can again be explained by the fact that for higher σ^2 the phenomenon of preferential flow paths intensifies, thus leading to higher concentrations of the injected H^+ particles moving along these paths. This causes more dissolution inside these paths, thus contributing to faster growth of the hydraulic conductivity variance. Here again, the curves for all σ_0^2 values assume a power law shape after a significant enough number of particles have entered the field.

215 References

- Atkins, P. and De Paula, J.: Atkins' Physical Chemistry, Macmillan Higher Education, 2006.
- Gouy, G.: Sur l'energie utilisable, Journal de Physique Theorique et Appliquee, https://doi.org/10.1051/jphystap:018890080050101, 1889.
- Kloeden, P. E.: Numerical solution of stochastic differential equations, Applications of mathematics, Springer, Berlin, 1992.
- Kondepudi, D. and Prigogine, I.: Modern Thermodynamics: From Heat Engines to Dissipative Structures, John Wiley and sons Ltd., 1998.
- Kreft, A. and Zuber, A.: On the physical meaning of the dispersion equation and its solutions for different initial and boundary conditions, Chemical Engineering Science, 33, 1471–1480, https://doi.org/https://doi.org/10.1016/0009-2509(78)85196-3, 1978.
 - Onsager, L.: Reciprocal Relations in Irreversible Processes. I., Phys. Rev., 37, 405–426, https://doi.org/10.1103/PhysRev.37.405, 1931.
 - Perez, L. J., Hidalgo, J. J., and Dentz, M.: Reactive Random Walk Particle Tracking and Its Equivalence With the Advection-Diffusion-Reaction Equation, Water Resources Research, 55, 847–855, https://doi.org/https://doi.org/10.1029/2018WR023560, 2019.
- 225 Risken, H.: The Fokker-Planck Equation: Methods of Solution and Applications, Springer Series in Synergetics, Springer Berlin Heidelberg, 1996.
 - Shavelzon, E. and Edery, Y.: Shannon entropy of transport self-organization due to dissolution–precipitation reaction at varying Peclet numbers in initially homogeneous porous media, Hydrology and Earth System Sciences, 28, 1803–1826, https://doi.org/10.5194/hess-28-1803-2024, 2024.